Study on Advanced Internal Cooling Technologies for the Development of Next-Generation Small-Class Aircraft Engines

Shu Fujimoto
e-mail: syuu_fujimoto@ihi.co.jp

Yoji Okita

IHI Corporation,
Tokyo 190-1297, Japan

Yoshitaka Fukuyama

Takashi Yamane

Fujio Mimura

Masahiro Matsushita

Japan Aerospace Exploration Agency,
Tokyo 182-8522, Japan

Toyoaki Yoshida
Tokyo University of Agriculture and Technology,
Tokyo 184-8588, Japan

An innovative internal cooling structure named multislot cooling has been invented for high-pressure turbine (HPT) nozzles and blades. This cooling structure has been designed to be simple and inexpensive and to exhibit good cooling performance. In order to confirm the cooling performance of this structure, test pieces of dummy turbine nozzles were manufactured. Three geometric parameters (width of slots, overall height of cooling channel, and height of jet impingement) are associated with these test pieces. The cooling performance tests were conducted by using these test pieces for several Reynolds numbers of the mainstream hot gas $[2.2\times10^5-3.4\times10^5]$ *and cooling airflow* $[3\times10^3-1\times10^4]$*. Infrared images of the heated surfaces of the test pieces were captured for every Reynolds number in the tests, and then the distributions of the cooling effectiveness were obtained. Simultaneously, the pressure losses were measured. This paper describes the hot gas flow tests performed to confirm the effects of the geometric parameters on the cooling performance and pressure loss, and to obtain data of Nusselt number and pressure loss coefficient for the design of turbine nozzles in the future by applying this new cooling structure to next-generation small-class aircraft engines. Additionally a preliminary analysis of airfoil cooling was performed to evaluate both cooling performance of conventional impingement cooling and multislot cooling when applied to a HPT nozzle. As a result it was found that the multislot cooling is well applicable to cooling of HPT airfoils.* [DOI: 10.1115/1.3151602]

1 Introduction

In recent years, the operating temperatures of gas turbines have continuously increased with improvements in their thermal efficiency. The turbine inlet temperatures of gas turbines reach up to several hundred degrees above 1000°C. Under these high-temperature conditions, metallic turbine parts need to be cooled so that the materials do not exceed their service temperature limits. Because the high-pressure air generated by the compressor is used for turbine cooling, the consumption of cooling air influences the efficiency of the engine immediately.

Currently in Japan, the Research and Technology Development in Japanese Environmentally Compatible Engine for Small Aircraft Project (ECO project) was started in 2003 as a 7 year project [1,2]. One of objectives of this project is to establish advanced technology required for next-generation small aircraft. In the ECO project, an innovative internal cooling structure named multislot cooling has been invented for application in high-pressure turbine nozzles and blades. This cooling structure is similar to the 180 deg turn of the serpentine cooling channel. The most significant difference between the two structures is that the cooling air flows between the pressure and suction sides in the multislot cooling channel (see Fig. 3).

Serpentine cooling channels are widely applied to thermal equipments and particularly to the cooling of turbine blades. Accordingly, several studies have been conducted on the 180 deg turn of serpentine cooling channels. Metzger et al. [3,4] first studied the overall heat transfer properties and pressure loss in the 180 deg turns in smooth rectangular serpentine channels by varying the diverter location and the turn clearance at the turn. Chyu [5] presented the heat transfer results in both the two- and three-pass channels with 180 deg turns. They showed that the heat transfer coefficient at the first turn attains thermally developed conditions. Han et al. [6], Ekkad et al. [7,8], Wang et al. [9], and Mochizuki et al. [10] investigated the influence of the rib attached on the channel wall. Nakayama et al. [11] measured the fluid flow in stationary two-pass channels with a sharp 180 deg turn by using a laser Doppler velocimeter (LDV) and investigated the influence of the size of the turn clearance on the flow structure.

This paper describes the new internal cooling structure named the "multislot cooling structure," which has been newly developed for application in high-pressure turbine nozzles of the three-dimensional geometry, and the result of the cooling performance test is described.

2 Cooling Structure of HPT Nozzle

2.1 Conventional Cooling Structure. HPT nozzles are located upstream of HPT rotor blades and downstream of a combustor. The function of the nozzles is to increase the speed of the main combustion gas and to turn it toward an appropriate direction. Therefore, HPT nozzles must be cooled because they are exposed to the high-temperature main gas flow. Figure 1 shows the cross-sectional diagram of the conventional cooling nozzle [12]. Impingement cooling is generally applied to conventional HPT nozzles. This impingement cooling archives high heat transfer by jet impingement on the inner wall of the turbine nozzles. Impingement inserts, which have a large number of small cooling holes, are assembled in the HPT nozzles. Bypass air from the exit of the high-pressure compressor (HPC) is introduced into the inserts and passes through cooling holes; finally, the air jets impinge on the inner wall of the turbine nozzles (impingement cooling). Figure 2 shows a schematic of the cooling flow in the conven-

Contributed by the International Gas Turbine Institute of ASME for publication in the JOURNAL OF TURBOMACHINERY. Manuscript received December 25, 2008; final manuscript received January 28, 2009; published online April 7, 2010. Review conducted by David Wisler. Paper presented at the ASME Turbo Expo 2008: Land, Sea and Air (GT2008), Berlin, Germany, June 9–13, 2008.

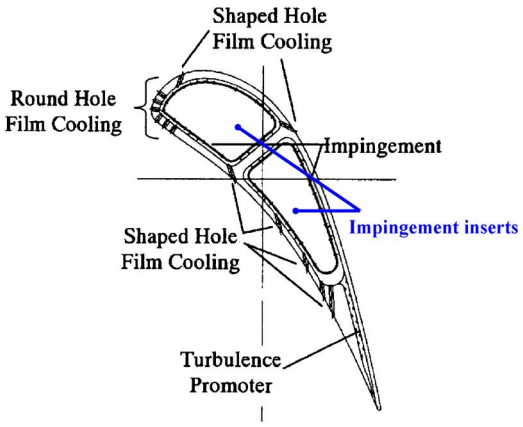

Fig. 1 Cross-sectional drawing of the conventional cooling nozzle [12]

tional cooling nozzle. In addition, film cooling holes are formed on the turbine wall; the cooling air used by impingement cooling is discharged into the main high-temperature gas flow, and the outer walls of the HPT nozzles are cooled. This prevents the direct conduction of the heat of the high-temperature flow from the main gas flow to the nozzle wall.

This conventional cooling structure has several drawbacks. The first drawback is that this structure requires additional components "impingement inserts," which are rather expensive. The second one is that the manufacturing of the turbine nozzles (the smaller jet engines), in which impingement inserts are installed, is considerably difficult or impossible. The third one is that a bowed nozzle, whose profile along the radial direction is bowed, is effective in reducing the pressure loss in the main gas flow (see Fig. 3(*a*)); however, impingement inserts cannot be applied to such nozzles.

Despite these drawbacks, HPT nozzles with impingement inserts have been installed in many jet engines and industrial gas turbines. This is because this cooling structure exhibits a considerably high cooling performance and, moreover, its pressure loss is significantly less. Because the cooling air is driven by the small difference in pressure between the exit of the HPC and the main gas flow inlet of the turbine, it is very important that the pressure loss in the HPT nozzle cooling structure is low. Thus, impingement inserts are suitable for HPT turbine nozzle cooling.

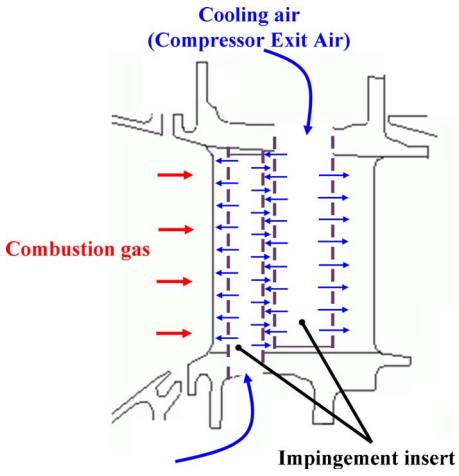

Fig. 2 Schematic of the cooling flow in the conventional cooling nozzle

2.2 Multislot Cooling Structure. As described previously, the ECO engine project requires improvement with regard to environmental compatibility for future advanced engines and reduction in the direct operation costs (DOCs); in other words, improvement in the engine efficiency and reduction in the manufacturing costs are required.

We have started to develop a new cooling structure whose cooling performance is almost equivalent to that of the impingement-insert-type cooling structure; this structure also eliminates some of the drawbacks mentioned previously.

The developmental targets of this new cooling structure are as follows:

i. reduction in the manufacturing costs by avoiding additional parts, that is, impingement inserts
ii. cooling performance equivalent to that of the impingement-insert-type cooling structure and reduction in the pressure loss
iii. improvement in the engine efficiency by adopting the bowed nozzle (reduction in the aerodynamic loss in the main gas flow)

We invented a new cooling structure (multislot cooling) that satisfies the abovementioned targets (see Fig. 3). Basically, this cooling structure has two cooling passages. In the first cooling passage, the nozzle surface of the leading edge (LE) neighborhood is cooled; in the second passage, the nozzle surface of the mid chord and trailing edge (TE) neighborhood is cooled. Each cooling passage has slots, which are formed by setting the ribs alternately so that the cooling air efficiently cools on the wall of the airfoil (see Fig. 3(*b*)).

Next, we present the cooling air flow lines in the cooling passage. First, the cooling air is introduced from the inlet at the tip or hub. Although it is almost indifferent whether cooling air is introduced from the tip or hub face, Fig. 3(*a*) shows that the cooling air is introduced from only the inlet at the tip face. In this case, the cooling air introduced at the inlet flows in a direction toward the hub from the tip. A part of this cooling flow gradually diverges through a slot, as described previously, and cools the wall of the airfoil. This diverged cooling air flows into the next slot and then cools on the wall. Finally, the cooling air used for cooling is discharged into the main gas flow through film holes and then used for film cooling.

In this cooling structure, the same cooling air is repeatedly used for cooling; thus, high heat transfer coefficient is expected to be achieved for small amounts of cooling air. In addition, because the cross-sectional area of a slot is large, the pressure loss at a slot and at the overall passage, including the slots, is expected to be very low.

The largest manufacturing difficulty of airfoils with multislot cooling is whether the ceramic core can be manufactured or not. In 2006, we manufactured the ceramic cores and precision casting nozzles with multislot cooling structures by way of try. As a result, we confirmed that there was no major problem in production of the airfoils with multislot cooling. Furthermore, we confirmed that the weight of nozzles with multislot cooling was slightly heavier than those with conventional impingement cooling, but there was almost no problem in the weight increase from a DOC standpoint.

In this study, in order to confirm whether or not the newly-invented cooling structure satisfies the performance requirements (cooling effectiveness and pressure loss), test pieces that simulate the part, which is the midchord and TE neighborhood of the HPT nozzle, were manufactured and tested in the hot gas flow (see Fig. 3(*b*)).

3 Cooling Performance Test

3.1 Test Facility and Rig. This test was conducted by using the test facility and rig in the Japan Aerospace Exploration

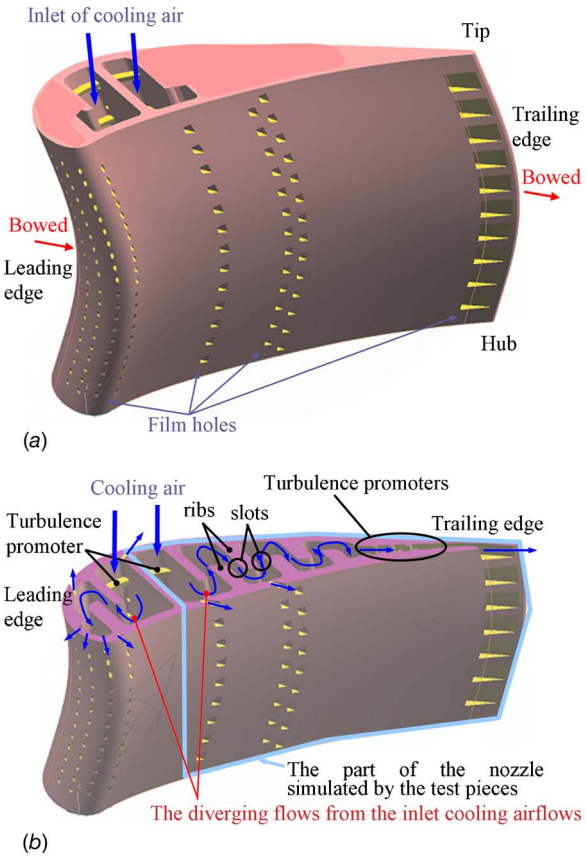

Fig. 3 Image of a turbine nozzle to which the multislot cooling structure can be applied: (*a*) overall view of a turbine nozzle and (*b*) cut model of turbine nozzle

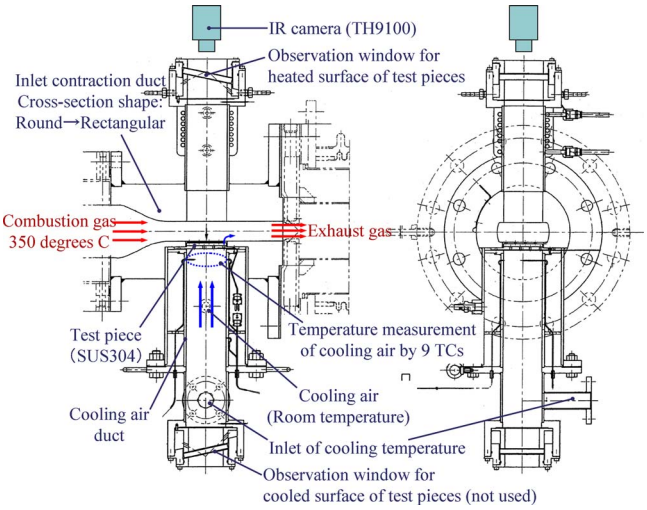

Fig. 5 Schematic of the test rig for the basic cooling performance test

Agency (JAXA). The schematic of the test facility is shown in Fig. 4, and the schematic of the test rig is shown in Fig. 5. Two flow piping systems exist in this test rig. The first system is the main gas flow system that passes through the inlet orifice flow meter, combustor, inlet contraction duct, and test section. The other system is the cooling air flow system that passes through the mass flow meter, cooling air duct, and test piece. The cooling air flow discharges from the test piece through round holes and then into the main gas flow. The main gas flow heats the test piece, which is then cooled by the cooling air flow.

Temperature probes are installed at the inlet of the test section in order to measure the inlet gas temperature. The inlet static pressure is measured. Nine thermocouples (TCs) are installed in the cooling duct in order to measure the cooling air temperature. The static pressure is measured in the cooling duct. An infrared (IR) camera (NEC Sanei TH9100 series, two-dimensional micro bolometer) is set facing the heated surface of the test piece through the observation window in order to measure its temperature field. In addition, the black paint is applied on the heated surfaces of the test pieces, and two thermocouples are placed on the heated surface of the test piece to calibrate its IR temperature field by using these TC temperatures.

3.2 Test Piece. The test pieces were manufactured not only to confirm whether or not this new cooling structure can exhibit sufficient performance required for HPT cooling nozzles but also to obtain data for the cooling design (see Fig. 6). As previously mentioned, test pieces simulate the nozzle surface of the midchord and TE neighborhood.

The most significant difference between this test piece and the actual turbine nozzle is that one side of the test piece is heated, the other side is not heated; on the other hand, in the case of HPT nozzles the both sides are heated. The test pieces have three geometric parameters: slot width (W), impingement height (H), and overall height of passage (Z). The scale of the test piece is twice

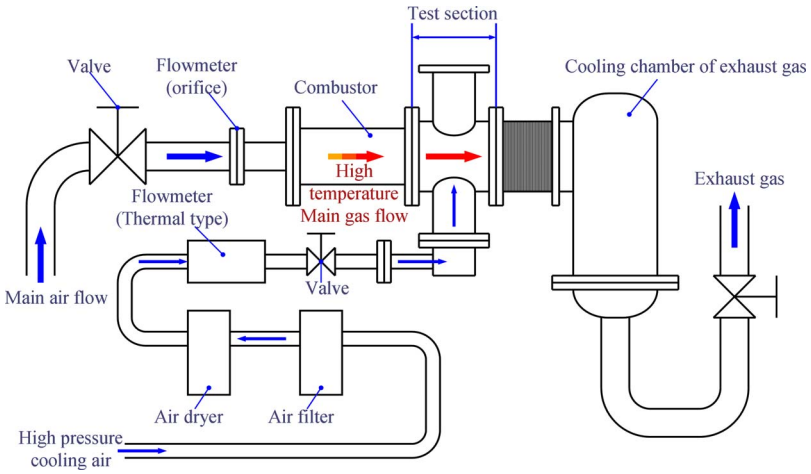

Fig. 4 Schematic of the test facility for the basic cooling performance test

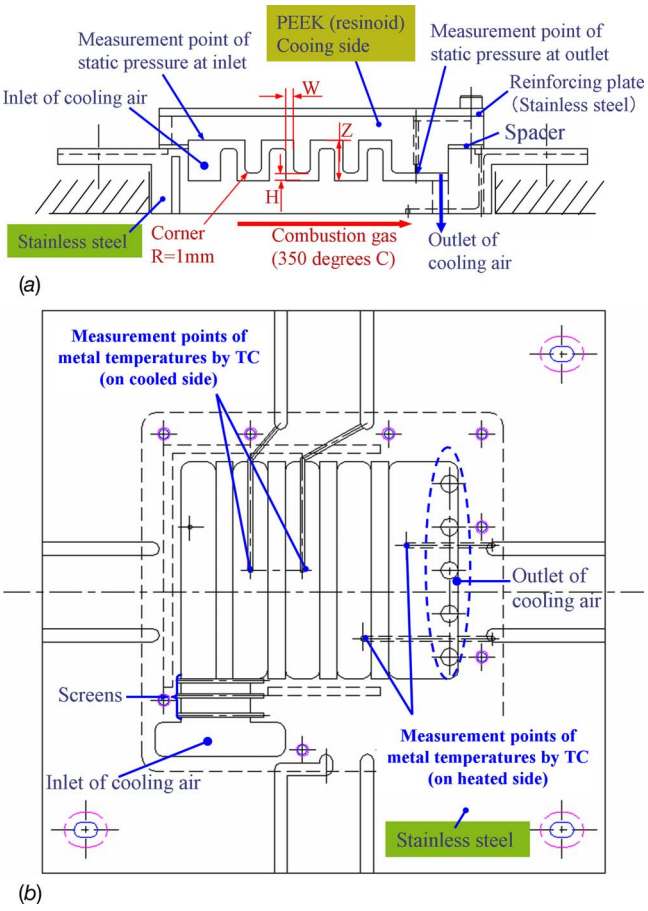

Fig. 6 Schematic of a test piece for the basic cooling performance test: (*a*) side view of a test piece and (*b*) top view of a test piece (a part of stainless steel)

that of the HPT nozzles of a baseline engine.

In addition, the static pressure is measured at the adjacent passage of the inlet and exit of the cooling air in the test piece. These pressure data are utilized to estimate the pressure loss of the cooling passage in the test piece.

Table 1 Test condition (a) Main gas flow conditions, (b) cooling air flow conditions, and (c) other conditions

(a) Test condition (main gas flow)		No. 1	No. 2
Mass flow rate	w_g (kg/s)	0.3	0.45
Mean velocity	V_g (m/s)	100	120
Inlet temperature	T_g (°C)	350	
Inlet pressure	P_g (MPa)	0.13	0.16
Reynolds number	Re_g	2.2×10^5	3.4×10^5
(b) Test condition (cooling air)		Minimum	Maximum
Mass flow rate	w_c (kg/s)	0.003	0.01
Inlet temperature	T_c (°C)	10	20
Inlet pressure	P_c (MPa)	0.14	0.3
Reynolds number	Re_{cW}	3.0×10^3	1.0×10^4
(c) Test condition (other conditions)		Minimum	Maximum
Temperature ratio	T_g/T_c	2.1	2.2
Biot number	Bi	0.12	0.22

Table 2 Geometric parameter of the test pieces

Geometric Parameter		Small	Base	Large
Width of slots	W (mm)	1	2	3
Overall height of cooling channel	Z (mm)	6	10	14
Height of jet impingement	H (mm)	1	2	4

3.3 Test Condition. Table 1 shows the test conditions, that is, the main gas flow, cooling air flow and other conditions. The main gas flow conditions have two levels, Nos. 1 and 2.

Table 2 shows the geometric parameters the in tests: slot width (W), impingement height (H), and overall height of passage (Z).

For the recent small and middle class aircraft engines, the main gas flow Reynolds number at the turbine inlet is approximately 1×10^5–5×10^5, which at the turbine exit is the order of 10^6, the cooling airflow Reynolds number of the turbine nozzle Re_{cW} is approximately 5×10^3–1×10^4. Regarding other conditions, the temperature ratio T_g/T_c is approximately 2.0–2.2, and the Biot number Bi is approximately 0.1–0.4. The dimensional ratio of slots is $W/H=1$.

According to above parameters of the test and real engines conditions, the cooling airflow conditions of the tests cover those of the real engines. The hot gas flow conditions of the tests are included in those of the real engines. Therefore both the main gas flow and cooling airflow conditions of the tests are almost equivalent to those of the real engines.

3.4 Uncertainty. In our previous study [13], the average uncertainty in the measured cooling effectiveness was estimated to be ±5.4% for a confidence of 95%. The results in this study retain the same level of accuracy.

Furthermore the metal temperature on the uncooled surrounding areas of the test piece is high; hence, it should be considered that the heat flux from these areas is not negligible, and heat conduction error must be estimated to obtain the accurate cooling effectiveness. The local cooling effectiveness is calculated at the center ($\%x=45\%$, $\%y=50\%$) of the test pieces in the next section 4.1. The conduction bias of the local cooling effectiveness at the center of the test pieces is estimated to be about −8.6% at the maximum by heat transfer analyses and this is relatively low. For reference, that at the edge of the test pieces is estimated about −34% at the maximum. This is very high, therefore not negligible.

4 Test Results and Discussion

As mentioned previously, the cooling performance tests were conducted to confirm the basic cooling performance of the newly-invented cooling structure, multislot cooling. The results of these tests are given as follows.

4.1 IR Images and Cooling Effectiveness. In this test, IR images of the heated surfaces of the test pieces were captured. These IR images were correlated by using the temperatures of two thermocouples on the heated surface in order to obtain more precise temperature fields on the heated surfaces. Figure 7 shows an example of the temperature field captured by the IR camera under typical conditions. As mentioned previously, the metal temperature on the uncooled surrounding areas of the test piece is high and the heat flux from these areas is not negligible at the edge of the test pieces. In order to obtain the heat transfer coefficient on the test pieces, back analyses of the heat transfer are required, as shown in Sec. 4.3.

Figure 8 shows the distributions of the cooling effectiveness at $\%y=20\%$, 50%, and 80% of the temperature field shown in Fig. 7. As mentioned previously, because heat flows from uncooled surrounding areas into the test region, the cooling effectiveness at small values of $\%x$ is low, and it is the highest around $\%x$

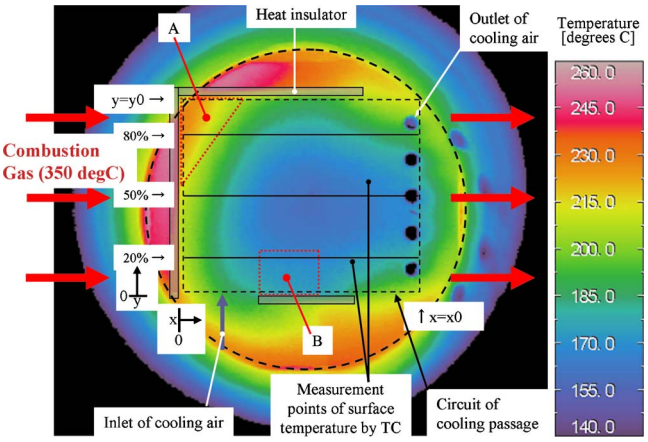

Fig. 7 Example of the temperature field captured by the IR camera under typical conditions

=50%. The cooling effectiveness at $\%x=60-80\%$ is lower than that at $\%x=50\%$. This is because the larger the value of $\%x$ is, the higher the temperature of cooling air becomes in the cooling passage due to the heat transfer from the metal to the cooling air.

According to a previous study (visualization of computational fluid dynamics (CFD) and particle image velocimetry (PIV)) [14], in areas A and B in Fig. 7, the cooling airflow is insufficiently provided; thus, it was expected that the metal surfaces on areas A and B were insufficiently cooled, and their temperatures were higher than those of the other areas. However, the surface temperature on area A was high, as predicted. However, the temperature on area B was not as high as predicted.

4.2 Cooling Performance Dependency on Geometric Parameters. Several tests were conducted under various geometric parameters (see Table 2). IR images of the heated surfaces of the test pieces were captured, and the pressure losses in them were measured for every test. The local cooling effectiveness at the center ($\%x=45\%$, $\%y=50\%$) of the test pieces was calculated, and the pressure loss coefficients of the entire cooling passage were obtained in order to confirm the dependence of the geometric parameters on the cooling performance and pressure loss. For calculating the local cooling effectiveness, the air temperature in the cooling duct (T_c) was used as the cooling air temperature along

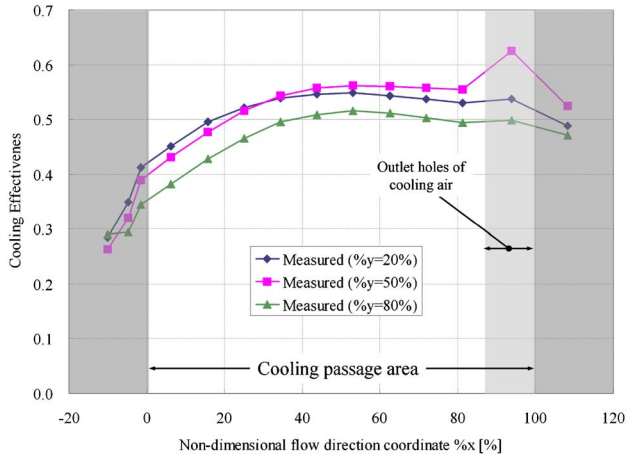

Fig. 8 Example of the cooling effectiveness distribution on a test piece

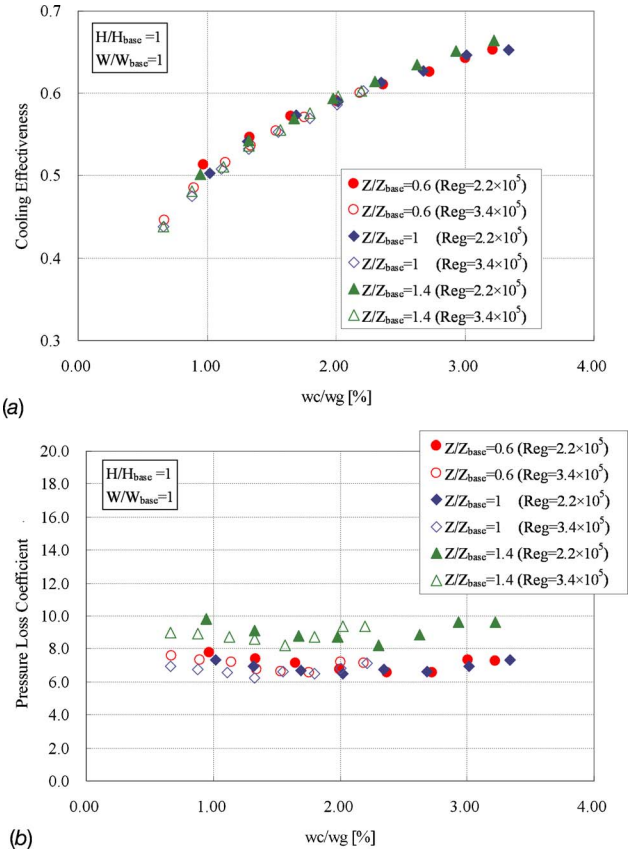

Fig. 9 Dependence on the overall height of the cooling passage (*Z*): (*a*) local cooling effectiveness at the center of the test piece and (*b*) pressure loss coefficient of the entire cooling passage

with the local heated surface temperature (T_{wg}).

For comparison of the dependence on each geometric parameter, one parameter was changed under the base values of the other two parameters.

4.2.1 Dependence on Overall Height of the Cooling Passage (Z). The cooling effectiveness does not depend on the ratio of the overall cooling passage height Z/Z_{base} for all the Reynolds numbers of the cooling airflow (refer to Fig. 9(*a*)). The pressure loss coefficient at $Z/Z_{base}=0.6$ is almost as high as that at $Z/Z_{base}=1$. On the other hand, the pressure loss coefficient at $Z/Z_{base}=1.4$ is higher than that at $Z/Z_{base}=1$ and 0.6 by approximately 20% (refer to Fig. 9(*b*)). Regarding pressure loss, it appears that the pressure loss at $Z/Z_{base}=1.4$ is high because the length of the entire cooling passage, that is, the total friction loss becomes larger than that in the other cases. The parameter Z corresponds to the distance between the pressure and suction surface of the airfoil, which is varied with the chordwise location of the airfoil. Thus the pressure loss of the multislot cooling is the difference in accordance with the chordwise location of the airfoil.

4.2.2 Dependence on the Impingement Height (H). Because cost reduction in the tests is required to be reduced, and the cooling effectiveness does not depend on Z/Z_{base}, the parts of the test piece were shared, and the impingement height H/H_{base} was changed only by replacing the spacers. Refer to Fig. 6(*a*). Therefore, $Z/Z_{base}=0.9$ when $H/H_{base}=0.5$ and $Z/Z_{base}=1.2$, when $H/H_{base}=2$. Z/Z_{base} of these cases are sufficiently close to 1.

When the ratio of the jet impingement height H/H_{base} becomes 0.5 (2.0), the cooling effectiveness is increased (decreased) by 0.02 through 0.03 for all the Reynolds numbers of the cooling

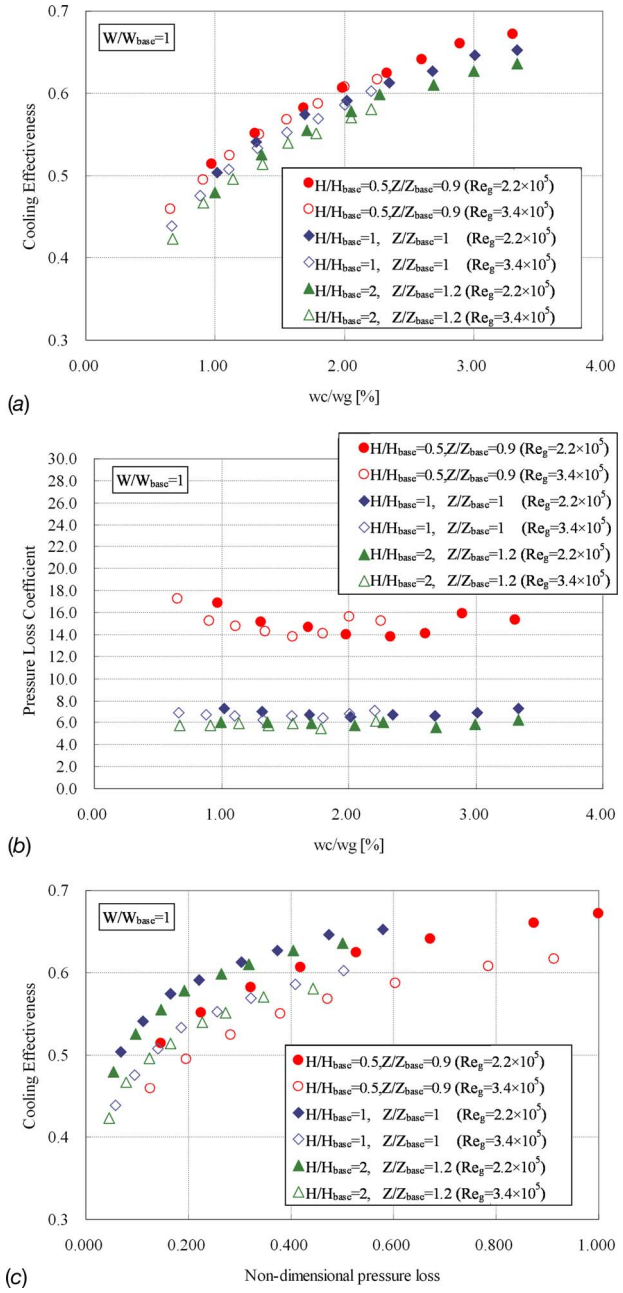

Fig. 10 Dependence on the impingement height (H). (*a*) Local cooling effectiveness at the center of the test piece. (*b*) Pressure loss coefficient of the entire cooling passage. (*c*) Cooling effectiveness versus nondimensional pressure loss.

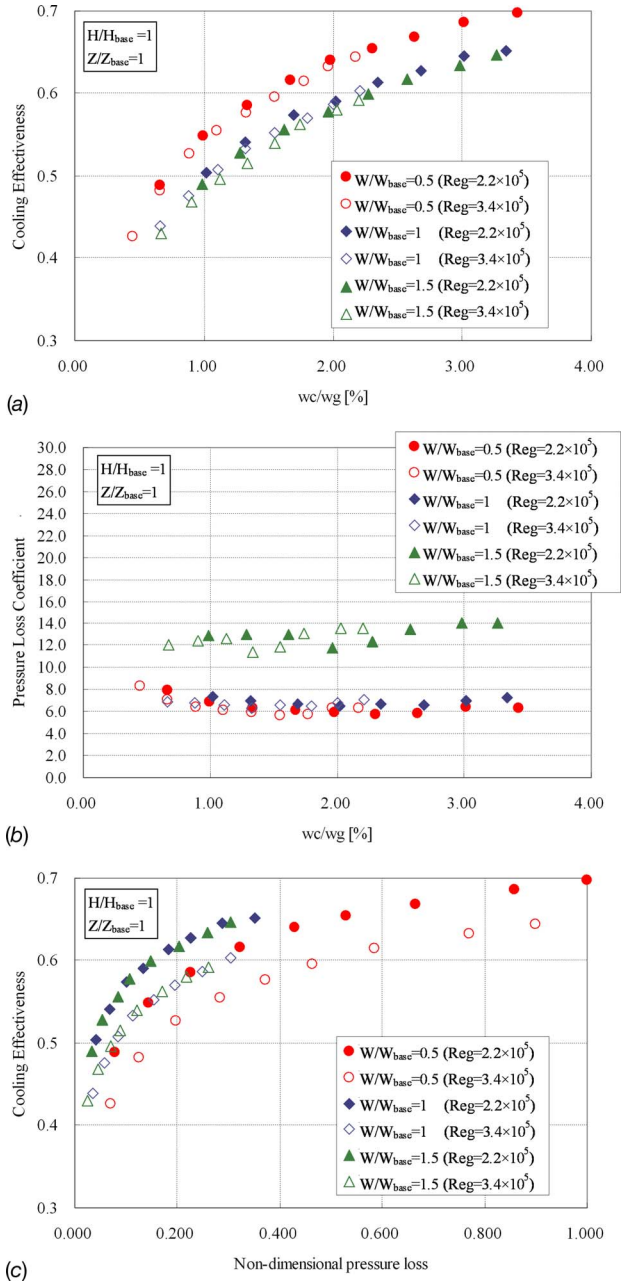

Fig. 11 Dependence on the impingement slot width (W). (*a*) Local cooling effectiveness at the center of the test piece. (*b*) Pressure loss coefficient of the entire cooling passage. (*c*) Cooling effectiveness versus nondimensional pressure loss.

airflow (refer to Fig. 10(*a*)). When the ratio of the jet impingement height H/H_{base} becomes 0.5, the pressure loss coefficient is increased to twice as much as that of $H/H_{base}=1$, and when H/H_{base} becomes 2.0, its coefficient is decreased by approximately 10% ever though Z/Z_{base} becomes slightly large (refer to Fig. 10(*b*)). The variation in cooling effectiveness with respect to pressure loss is shown in Fig. 10(*c*). Pressure loss was nondimensionalized by the highest pressure loss among all cases. Considering both the cooling effectiveness and the pressure loss, the cooling structure of the geometric parameter $H/H_{base}=1$ and 2 appears to be reasonable when $W/W_{base}=1$ and $Z/Z_{base}=1$.

4.2.3 Dependence on the Impingement Slot Width (W). When $W/W_{base}=0.5$, the cooling effectiveness is considerably higher than that at $W/W_{base}=1$ by 0.05–0.06 for all the Reynolds numbers of the cooling airflow (refer to Fig. 11(*a*)). This is because the velocity of the impingement jet is twice that at $W/W_{base}=1$ owing to the half width of the slots, and the test piece is cooled very effectively by impingement cooling; however, the amount of cooling air cannot be reduced by half for the same cooling effectiveness. The cooling effectiveness at $W/W_{base}=1.5$ is slightly lower than that at $W/W_{base}=1$. The pressure loss coefficient at $W/W_{base}=0.5$ is almost similar to that at $W/W_{base}=1$. The pressure loss coefficient at $W/W_{base}=1.5$ is almost twice that at $W/W_{base}=1$ (refer to Fig. 11(*b*)). The variation in cooling effectiveness with respect to pressure loss is shown in Fig. 11(*c*). Pressure loss was nondimensionalized by the highest pressure loss among all cases. The pressure loss at $W/W_{base}=0.5$ is approximately thrice that at $W/W_{base}=1$. The pressure loss at W/W_{base}

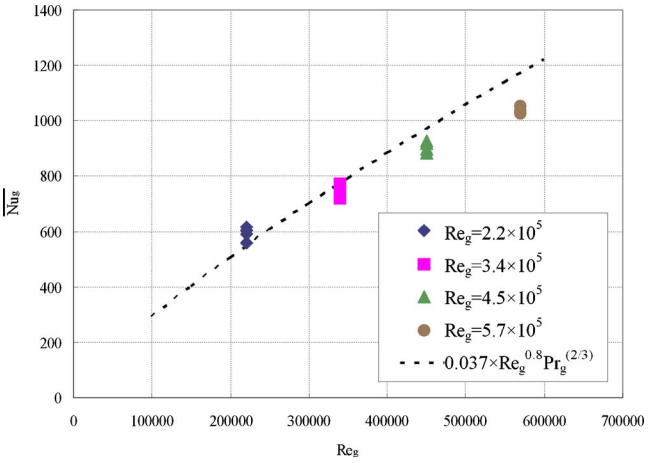

Fig. 12 Averaged Nusselt number of the heated surfaces of the test pieces $\overline{Nu}_g$ versus Reynolds number Re_g

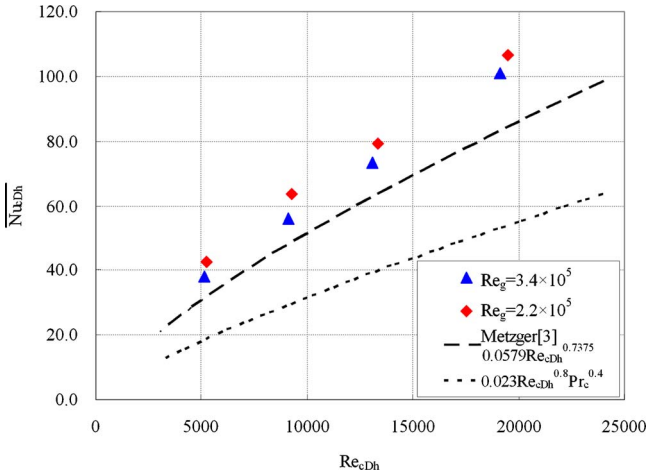

Fig. 14 Averaged Nusselt number of multislot cooling $\overline{Nu}_{cD_h}$ versus Reynolds number Re_{cD_h}

=1.5 is lower than that at $W/W_{base}=1$ by approximately 10%. Considering both the cooling effectiveness and pressure loss, the cooling structure for the geometric parameter at $W/W_{base}=1$ and 1.5 appears to be reasonable when $H/H_{base}=1$ and $Z/Z_{base}=1$.

4.3 Averaged Nusselt Number of the Multislot Cooling Structure. A back analysis of the heat transfer was carried out to obtain the averaged Nusselt number of the multislot cooling structure whose geometric parameters were the width of slots $W=2$ mm, overall height of cooling channel $Z=10$ mm, and height of jet impingement $H=2$ mm. These parameters are the typical ones.

First, the averaged Nusselt number on the heated surface was obtained by the back analysis by using the basic impingement cooling test piece. The characteristic length of Reynolds number is the flow-wise length of the test pieces L, 84 mm. The heat transfer coefficient on its cooled surface was obtained by using the correlation formula [15]. The averaged Nusselt number on the heated surface of the test pieces is shown in Fig. 12. For reference, averaged Nusselt number correlation of turbulent flow on the flat plate, $\overline{Nu}_g=0.037\times Re_g^{0.8}\times Pr_g^{(2/3)}$ is plotted in Fig. 12. Second, the averaged Nusselt number on the cooled surface of the multislot cooling test piece was obtained by back analysis by using the heat transfer coefficient on the heated surface that was previously obtained by the back analysis. The variation in the averaged Nusselt number of the multislot cooling structure with respect to the Reynolds number Re_{cW} is shown in Fig. 13.

In order to compare our test results with the experimental results presented by Metzger et al. [3,4], the graphs of the Nusselt number and pressure loss coefficient were replotted by using the hydraulic diameter D_h as the characteristic length of the Reynolds number. There are some differences between the two cooling passages. In this study, the aspect ratio $[y0:W]$ of the multislot cooling passage on the cross section is 25, which is very high, although that of Metzger's 180 deg turn of the serpentine passage is 0.4, which is very low. The flow diverter of Metzger's passage is thinner than that of the multislot passage in our study. The variation in the averaged Nusselt number of the multislot cooling structure with respect to the Reynolds number Re_{cD_h} is shown in Fig. 14. For reference, averaged Nusselt number correlation of the fully developed turbulent flow in the circular duct (its diameter is D_h), $\overline{Nu}_{cD_h}=0.023\times Re_{cD_h}^{0.8}\times Pr_c^{0.4}$ is plotted in Fig. 14. The variation in the pressure loss coefficient per 180 deg turn of the multislot cooling structure with respect to the Reynolds number (Re_{cD_h}) is shown in Fig. 15.

The averaged Nusselt number of the multislot passage is better than that of the 180 deg turn of Metzger's serpentine passage, although the pressure loss coefficient per 180 deg turn of the

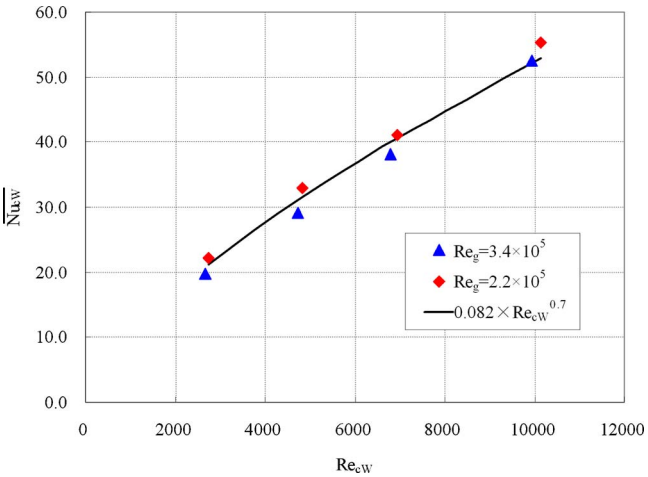

Fig. 13 Averaged Nusselt number of the multislot cooling $\overline{Nu}_{cW}$ versus Reynolds number Re_{cW}

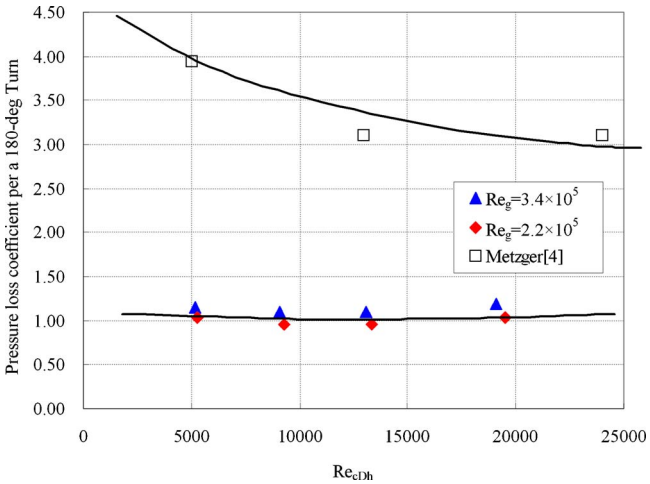

Fig. 15 Pressure loss coefficient per 180 deg turn of multislot cooling versus Reynolds number Re_{cD_h}

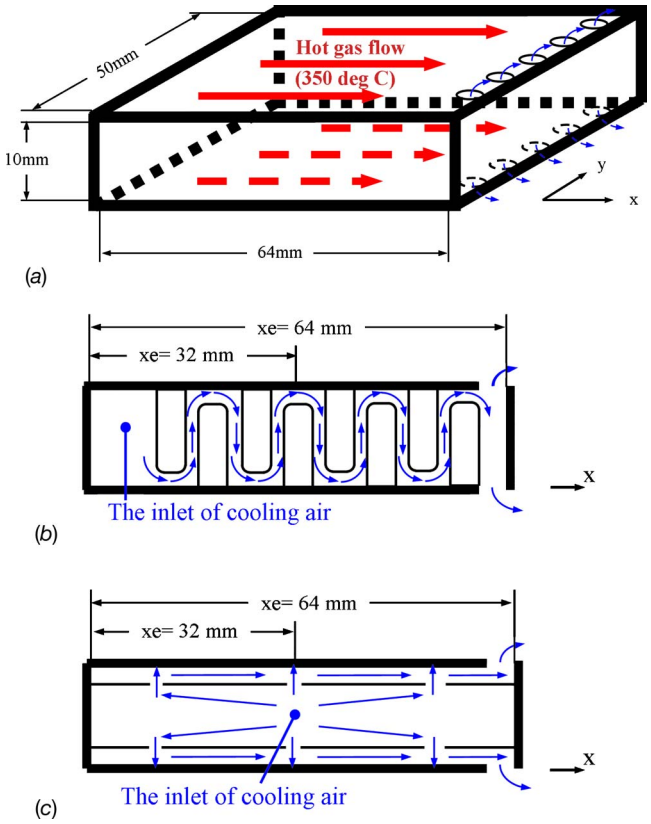

Fig. 16 Preliminary analysis models of airfoil cooling: (*a*) overall view, (*b*) cross-sectional drawing of multislot cooling, and (*c*) cross-sectional drawing of conventional impingement cooling

multislot passage is approximately thrice as low as that of Metzger's serpentine passage. This is because the endwalls of Metzger's cooling passage are close to each other; therefore, the secondary flow loss develops further, and the pressure loss becomes large. On the other hand, the endwalls of the multislot cooling structure are far apart from each other; therefore, the pressure loss is very low when compared with its cooling performance.

5 Preliminary Analysis of Airfoil Cooling

A preliminary analysis of airfoil cooling was performed to evaluate both cooling performance of conventional impingement cooling and multislot cooling in applying to a HPT nozzle. Preliminary analysis models of airfoil cooling are shown in Fig. 16.

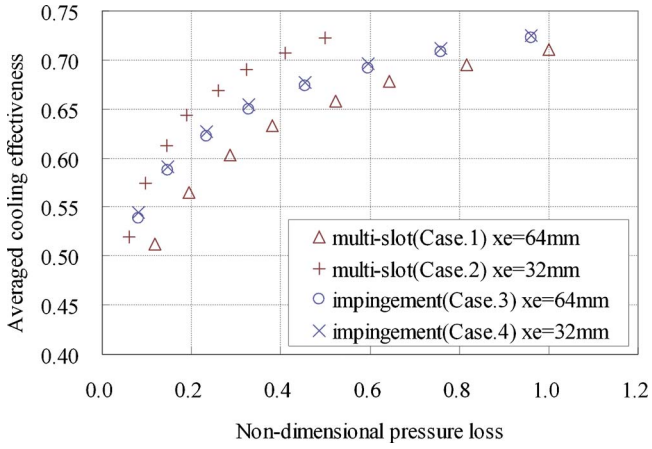

Fig. 17 Averaged cooling effectiveness $\bar{\eta}$ versus nondimensional pressure loss

5.1 Condition of Analysis. In this preliminary analysis, both of the upper and lower surfaces are exposed to the hot gas flow at 350°C, though only single surface was exposed to the hot gas flow in our experiments. Other four side walls are adiabatic.

The heat transfer coefficient at the heated surfaces, which was obtained at the hot gas flow test ($Re_g = 2.2 \times 10^5$, see Fig. 12) is used. The inlet cooling temperature is 20°C.

5.2 Geometric Parameter of Analysis Cases. All cases that were analyzed are shown in Table 3. The wall thickness of all surfaces is set to 2 mm. The cooling structures are built in the region of the $64 \times 50 \times 10$ mm^3 box.

5.3 Results and Discussion. The averaged cooling effectiveness $\bar{\eta}$ of case 1–4 was calculated using the averaged temperature of heated surfaces $\overline{T_{wg}}$, and their pressure losses were calculated against overall cooling passage, except for the exit holes. The variation in cooling effectiveness with respect to pressure loss is shown in Fig. 17. Pressure loss was nondimensionalized by the highest pressure loss of case 1.

Comparing case 1(multislot) to case 3(conventional impingement), whose performance estimation regions in the flow direction (*xe*) are 64 mm, the cooling effectiveness of case 1 is lower than that of case 3. Especially at low pressure loss (small amount of cooling airflow) region, the difference between the two cases is large. The reason is that the same cooling air is repeatedly used for impingement cooling at the turns for case 1, thus cooling air

Table 3 Geometric parameter of analysis cases

Case No.	Cooling structure	Geometry	Performance estimation region in flow direction (mm)	Nusselt number	Figure
1	Multislot cooling	$W=2$ mm $H=2$ mm $Z=10$ mm	$xe=64$	$0.082 \times Re_{cW}^{0.7}$	16(*b*)
2			$xe=32$		
3	Conventional impingement cooling	Hole diameter=2 mm Impingement height=3.5 mm No. of holes (*x*-direction)=3 No. of holes (*y*-direction)=5	$xe=64$	Florschuetz et al. [15]	16(*c*)
4		$Z=10$ mm	$xe=32$		

temperature becomes high at low pressure loss (small amount of cooling airflow) region. On the other hand, comparing case 2 (multislot) to case 4 (conventional impingement), whose performance estimation regions in the flow direction (xe) are 32 mm, the cooling effectiveness of case 2 is higher than that of case 4. The reason is that the number of the turns of case 2 is fewer than that of case 1, thus, the cooling temperature of case 2 does not become so high, and the pressure loss of case 2 is half as high as that of case 1, though the amount of cooling air for the entire analysis model required is more. In contrast, the pressure loss and cooling effectiveness of case 4 are almost the same as those of case 3, when the amount of cooling air for the entire analysis model is unchanged.

Each cooling structure, multislot and conventional impingement cooling, have their own characteristics. Thus it is important that the appropriate cooling structure is selected as requirement of cooling design. In minding these points, the multislot cooling is well applicable to cooling of HPT airfoils.

6 Conclusion

This paper deals with the cooling performance tests for several Reynolds numbers of mainstream hot gas and cooling airflow by using test pieces, which have three geometric parameters. In addition, the preliminary analysis of airfoil cooling was performed to evaluate both cooling performance of conventional impingement cooling and multislot cooling when applied to a HPT nozzle. We present the following findings.

1. Regarding two areas that lack cooling air (A and B), which were predicted by flow visualization by CFD and PIV, the surface temperature of area A is high, as predicted. However, the surface temperature of area B is not as high as predicted.
2. The pressure loss of the multislot cooling is difference in accordance with the geometric parameter Z, in the other words, the chordwise location of the airfoil.
3. Considering both cooling effectiveness and pressure loss, the cooling structure for the geometric parameters $H/H_{\text{base}}=1-2$ at $W/W_{\text{base}}=1$ or $W/W_{\text{base}}=1-1.5$ at $H/H_{\text{base}}=1$ appears to be reasonable.
4. It was confirmed that the pressure loss in the multislot cooling structure is very low when compared with its cooling performance against the 180 deg turn of the serpentine cooling passage in the study of Metzger et al. [3,4].
5. The preliminary analysis of airfoil cooling showed that each cooling structure, multislot and conventional impingement cooling, has its own characteristics. Thus it is important that the appropriate cooling structure is selected as a requirement of cooling design. In minding these points, the multislot cooling is well applicable to cooling of HPT airfoils.

Acknowledgment

The authors would like to express their thanks to the New Energy and Industrial Technology Development Organization (NEDO) and the Ministry of Economy, Trade and Industry (METI), who gave them the opportunity to conduct "Research and Development for Environmentally Compatible Engine for Small Aircraft (ECO Engine) Project."

Nomenclature

- Bi = Biot number, $h_g t_w/k_w$
- C_{pt} = pressure loss coefficient, $\Delta P_t/(0.5\times\rho_{ci}V_{ci}^2)$
- D_h = hydraulic diameter, $4WH/(2(W+H))$ (m)
- H = height of jet impingement (m)
- h = heat transfer coefficient (W/(m^2 K))
- k = thermal conductivity (W/(m K))
- L = flow-wise length of test pieces (m)
- $\overline{\text{Nu}_{cD_h}}$ = averaged Nusselt number of cooling air flow (characteristic length is D_h), hD_h/k_{ci}
- $\overline{\text{Nu}_{cW}}$ = averaged Nusselt number of cooling air flow (characteristic length is W), hW/k_{ci}
- $\overline{\text{Nu}_g}$ = averaged Nusselt number of hot gas flow (characteristic length is L), hL/k_g
- P = pressure (Pa)
- Pr = Prandtl number
- ΔP_t = total pressure loss (Pa)
- Re_{cD_h} = Reynolds number of cooling air flow (characteristic length is D_h), $\rho_{ci}V_{ci}D_h/\mu_{ci}$
- Re_{cW} = Reynolds number of cooling air flow (characteristic length is W), $\rho_{ci}V_{ci}W/\mu_{ci}$
- Re_g = Reynolds number of hot gas flow (characteristic length is L), $\rho_g V_g L/\mu_g$
- t_w = wall thickness (m)
- T = temperature (K)
- $\bar{T}$ = averaged temperature (K)
- V = mean velocity (m/s)
- w = mass flow rate (kg/s)
- W = width of slots (m)
- x, y = coordinates (m)
- $x0$, $y0$ = overall length of cooling passage (m)
- $\%x$, $\%y$ = nondimensional coordinates $\%x=x/x0$, $\%y=y/y0$
- xe = Performance estimation region in the flow direction (m)
- Z = overall height of cooling channel (m)
- η = cooling effectiveness, $(T_g-T_{wg})/(T_g-T_c)$
- $\bar{\eta}$ = averaged cooling effectiveness, $(T_g-\overline{T_{wg}})/(T_g-T_c)$
- μ = viscosity (Pa s)
- ρ = density (kg/m^3)

Subscripts

- base = medium value of geometric parameters
- c = cooling air in the cooling duct
- ci = cooling air at the inlet of a slot
- g = hot combustion gas
- t = total
- w = solid metal
- wc = at metal surface exposed to cooling air flow
- wg = at metal surface exposed to hot gas flow

References

[1] Funatogawa, O., Fujimura, T., and Kobayashi, K., 2006, "Research and Development of ECO engine," Journal of the Gas Turbine Society of Japan, **34**(3), pp. 18–23.

[2] Funatogawa, O., 2005, "Research and Technology Development in Japanese Environmentally Compatible Engine for Small Aircraft Project," 17th ISABE Conference, Paper No. ISABE2005-1010.

[3] Metzger, D. E., and Sahm, M. K., 1986, "Heat Transfer Around Sharp 180-deg Turns in Smooth Rectangular Channels," ASME J. Heat Transfer, **108**, pp. 500–506.

[4] Metzger, D. E., Plevich, C. W., and Fan, C. S., 1984, "Pressure Loss Through Sharp 180 deg Turns in Smooth Rectangular Channels," ASME J. Eng. Gas Turbines Power, **106**, pp. 677–681.

[5] Chyu, M. K., 1991, "Regional Heat Transfer in Two-Pass and Three-Pass Passages With 180-deg Sharp Turn," ASME J. Heat Transfer, **113**, pp. 63–70.

[6] Han, J. C., Chandra, P. R., and Lau, S. C., 1988, "Local Heat/Mass Transfer Distributions Around Sharp 180 deg Turns in Two-Pass Smooth and Rib-Roughened Channels," ASME J. Heat Transfer, **110**, pp. 91–98.

[7] Ekkad, S. V., and Han, J. C., 1995, "Local Heat Transfer Distributions Near a Sharp 180 Degree Turn of a Two-Pass Square Channel Using a Transient Liquid Crystal Image Technique," J. Flow Visualization Image Process., **2**, pp. 287–298.

[8] Ekkad, S. V., Pamula, G., and Santhiniketanam, M., 2000, "Detailed Heat Transfer Measurements Inside Straight and Tapered Two-Pass Channels With Rib Turbulators," Exp. Therm. Fluid Sci., **22**, (Issue 3–4), pp. 155–163.

[9] Wang, Z., Ireland, P. T., Kohler, S. T., and Chew, J., 1998, "Heat Transfer Measurements to a Gas Turbine Cooling Passage With Inclined Ribs," ASME J. Turbomach., **120**, pp. 63–69.

[10] Mochizuki, S., Murata, A., Shibata, R., and Yang, W.-J., 1998, "Detailed Measurements of Local Heat Transfer Coefficients in Turbulent Flow Through Smooth and Rib-Roughened Serpentine Passages With a 180° Sharp Bend,"

Int. J. Heat Mass Transfer, **42**, pp. 1925–1934.
[11] Nakayama, H., Hirota, M., Fujita, H., Yamada, T., and Koide, Y., 2006, "Fluid Flow and Heat Transfer in Two-Pass Smooth Rectangular Channels With Different Turn Clearances," ASME J. Eng. Gas Turbines Power, **128**, pp. 772–785.
[12] Yamawaki, S., 2001, "Verifying Heat Transfer Analysis of High Pressure Cooled Turbine Blades and Disk," Ann. N. Y. Acad. Sci., **934**, pp. 505–512.
[13] Yamawaki, S., Nakamata, C., Imai, R., Matsuno, S., Yoshida, T., Mimura, F., and Kumada, M., 2003, "Cooling Performance of an Integrated Impingement and Pin Fin Cooling Configuration," ASME Paper No. GT2003-38215.
[14] Maikusa, Y., Yoshida, T., Fujimoto, S., and Okita, Y., 2007, "Study on Visualization of Cooling Airflow in a Turbine Nozzle With Multiple Slot Cooling Configuration," Ninth International Symposium on Fluid Control, Measurement and Visualization(FLUCOME 2007), Paper No. 54.
[15] Florschuetz, L. W., Truman, C. R., and Metzger, D. E., 1981, "Streamwise Flow and Heat Transfer Distributions for Jet Array Impingement With Crossflow," ASME J. Heat Transfer, **103**, pp. 337–342.